Am J Cancer Res 2026;16(3):1102-1114
www.ajcr.us /ISSN:2156-6976/ajcr0171687

Original Article

UFM1 regulates ferroptosis in oral squamous cell carcinoma by stabilizing SLC7A11

Gang Li, Hongwei Yang, Jing Guo

Department of Prosthodontics, Shanxi Provincial People's Hospital, Taiyuan 030012, Shanxi, China

Received January 26, 2026; Accepted March 25, 2026; Epub March 25, 2026; Published March 30, 2026

Abstract: Oral squamous cell carcinoma (OSCC) is highly invasive malignancy with limited effective therapeutic strategies. Ubiquitin-fold modifier 1 (UFM1) is a ubiquitin-like molecule that has been implicated in several cancers; however, its role in ferroptosis within OSCC remains unclear. In this study, UFM1 was demonstrated to be upregulated in OSCC. UFM1 depletion suppressed proliferation and dissemination of OSCC cells and induced ferroptosis characterized by increased lipid peroxidation and Fe^{2+} accumulation. Mechanically, UFM1 deficiency significantly reduced SLC7A11 levels and sensitized cells to oxidative stress. Reintroduction of SLC7A11 rescued ferroptosis and restored cell survival in UFM1-deficient cells. *In vivo*, UFM1 depletion significantly inhibited tumor growth, reduced SLC7A11 expression, and increased lipid oxidation, as indicated by 4-hydroxynonenal (4-HNE) immunohistochemical staining. These findings suggest that UFM1 protects OSCC from ferroptosis by stabilizing SLC7A11 protein via UFMylation, thereby preventing its proteasomal degradation.

Keywords: UFM1, oral squamous cell carcinoma, SLC7A11, ferroptosis

Introduction

Oral squamous cell carcinoma (OSCC) represents the predominant subtype of head and neck squamous cell carcinoma (HNSC). HNSC is a refractory malignancy with limited therapeutic strategies [1, 2]. Although the five-year survival rate of OSCC has shown modest improvement, overall prognosis remains unsatisfactory, largely due to diagnosis at advanced stage, strong metastatic potential, and presence of intrinsic or acquired drug resistance [3-5]. This clinic situation underscores the urgent need to elucidate the underlying molecular mechanisms of OSCC and identify new therapeutic targets.

Ubiquitin-fold modifier 1 (UFM1), a conserved ubiquitin-like (UBL) molecule, mediates a distinct post-translational modification termed UFMylation [6, 7]. Analogous to the canonical ubiquitination cascade, UFM1 utilizes unique triad of enzymes (E1 UBA5, E2 UFC1, E3 UFL1) to covalently conjugate to lysine residues. UFM1 is involved in multiple cellular processes: UFM1 plays a critical role in ribosome-associated protein quality control by facilitating the clearance of aberrant nascent chains and maintaining endoplasmic reticulum (ER) homeostasis [8]. As a result, UFM1 deficiency leads to severe consequences, including neurodegeneration and impaired hematopoietic stem cell function in mammals [9, 10]. Dysregulation of UFM1 has also been implicated in human diseases. For instance, Yan et al. reported aberrant UFM1 accumulation in Alzheimer disease [11], while Jing et al. demonstrated that UFM1 depletion destabilizes NLRP3 and triggers inflammatory responses [12]. Emerging evidence further suggests that UFM1 is involved in tumorigenesis across multiple cancer types, including breast cancer and HNSC [13-16]. However, studies on the expression pattern, biological function, and underlying molecular mechanism of UFM1 in OSCC remains limited.

Ferroptosis is a regulated form of cell death characterized by iron dependence and lipid peroxidation. It functions as a tumor suppressor in cancer development [17]. Cancer cells often exhibit elevated iron levels and metabolic activ-

https://doi.org/10.62347/HTNW7529

ity, rendering them more susceptible to ferroptotic stress; therefore, ferroptosis may represent a potential therapeutic strategy [18]. Solute carrier family 7 member 11 (SLC7A11, also known as xCT) is a key component of the cystine/glutamate antiporter system (system Xc^-), which mediates cystine uptake for glutathione (GSH) synthesis and protects cells from oxidative stress [19]. In OSCC, SLC7A11 is frequently up-regulated and contributes to disease progression and chemoresistance [20, 21]. Studies in breast cancer have reported that SLC7A11 may serve as a target for UFM1-mediated modification [22]. However, the regulatory relationship between UFM1 and SLC7A11 in OSCC remains unclear.

In this study, we systematically investigated the role of UFM1 in OSCC through bioinformatics analyses, in vitro experiments, and in vivo models. UFM1 is significantly upregulated in OSCC and promotes tumorigenicity by enhancing resistance to ferroptosis in a SLC7A11-dependent manner.

Materials and methods

Clinical specimen collection

A total of 25 paired tumor tissues and adjacent non-cancerous tissues were collected from OSCC patients who underwent radical resection at Department of Prosthodontics, Shanxi Provincial People's Hospital during March 2024 and February 2025. Adjacent normal epithelial tissues were obtained at least 2 cm away from the tumor margin and were histologically confirmed to be free of malignant cells. All diagnoses of OSCC were confirmed by postoperative pathological examination. This study was approved by the Ethics Committee of Shanxi Provincial People's Hospital. None of the patients had received radiotherapy, chemotherapy, or immunotherapy prior to surgery. Patients with recurrent OSCC, a history of other malignancies, prior neoadjuvant therapy, or distant metastasis at initial diagnosis were excluded. Tissue samples were processed immediately after surgical resection: one portion was fixed in formalin for pathological analysis, while the remaining was snap-frozen in liquid nitrogen for further molecular analyses. All specimens were pathologically verified before inclusion in the study.

Cell culture and transfection

The human oral keratinocyte strain (HOK) and three OSCC cell lines (SCC-25, Cal27, Ca9-22) were purchased from American Type Culture Collection (ATCC, Manassas, VA, USA). All cell lines were authenticated by short tandem repeat (STR) profiling and tested negative for mycoplasma contamination using a PCR prior to experiments. Cells were cultured in their respective recommended media supplemented with 10% FBS and 1% penicillin/streptomycin under standard conditions.

Regarding gene silencing, Cal27 and Ca9-22 cells were seeded into suitable culture plates and allowed to adhere for 24 h. Small interfering RNA targeting UFM1 (si-UFM1: 5'-CCTGCTGCAACAAGTGCAATT-3') or scramble negative control (si-NC: 5'-UUCUCCGAACGUGUCACGU-3') was transiently transfected into cells using Lipofectamine 3000 reagent (Invitrogen, Carlsbad, CA, USA). As for SLC7A11 overexpression, the pcDNA3.1-SLC7A11 plasmid was constructed by GenePharma (Shanghai, China). Cells were harvested 48 h after transfection for subsequent experiments.

Cell proliferation assay

Cells were seeded into 96-well plates at a density of 2×10^3 cells per well in 100 μL complete culture medium. At the indicated time points (0, 24, 48, and 72 h), 10 μL of CCK-8 reagent (Solarbio, Beijing, China) was added to each well and incubated at 37°C for 2 h. The optical density (OD) at 450 nm was measured using a microplate reader to evaluate cell proliferation.

Colony formation assay

Cells were trypsinized, counted, and seeded into 6-well plates at a low density of 500 cell per well. Cells were cultured for 10-14 days, with culture medium replaced every 3 days. Subsequently, colonies were fixed with 4% paraformaldehyde and stained with 0.1% crystal violet (Sigma-Aldrich, St. Louis, MO, USA). Colonies containing more than 50 cells were counted manually.

Transwell migration and invasion assays

Cell migration and invasion assays were conducted using Transwell chambers with 8-μm

pore size membranes (Corning, Corning, NY, US). For invasion, the upper chambers were precoated with 50 μL of Matrigel (diluted 1:8 in serum-free DMEM) and incubated at 37°C for 4 h. Transfected cells (1×10^5) suspended in 200 μL of serum-free DMEM were seeded into the upper chamber, while 600 μL of DMEM containing serum was added to the lower chamber as a chemoattractant. After incubation for 24 h (migration assay) or 48 h (invasion assay), non-migrated cells on the upper surface of the membrane were gently removed using a cotton swab. Cells migrated or invaded to the lower surface were fixed with 4% paraformaldehyde and stained with crystal violet (0.1%). Five random fields per membrane were photographed under a microscope, and the number of cells were counted.

2',7'-dichlorofluorescin diacetate (DCFH-DA) staining for intracellular ROS detection

Intracellular reactive oxygen species (ROS) levels were measured using DCFH-DA (Sigma-Aldrich). Cells were seeded on coverslips in 24-well plates and cultured for 48 h. After washing with PBS, cells were incubated with 10 μM DCFH-DA diluted in serum-free medium at room temperature for 30 min. Subsequently, cells were washed three times with PBS, and fluorescence images were captured using an Olympus fluorescence microscope (excitation wavelength of 488 nm and emission wavelength of 525 nm).

Mitochondrial superoxide detection

Mitochondrial superoxide production was assessed using MitoSOX™Red reagent (Invitrogen, Carlsbad, CA. USA). Cells were treated with 5 μM MitoSOX™ Red at 37°C for 30 min in the dark. After incubation, cells were rinsed with PBS, and fluorescence intensity was measured using a fluorescence microscope and a microplate reader (excitation/emission: 510/580 nm).

Measurement of Fe^{2+}, MDA, and GSH levels

Intracellular Fe^{2+}, malondialdehyde (MDA), and GSH levels were quantified using commercial assay kits (Nanjing Jiancheng Bioengineering Institute, Nanjing, China) according to the manufacturer's instructions. The absorbance values were measured at 593 nm (Fe^{2+}), 532 nm (MDA), and 412 nm (GSH) using spectrophotometer. Concentrations were calculated based on the corresponding standard curves.

Transmission electron microscopy (TEM)

Cells were fixed using 2.5% glutaraldehyde, followed by post-fixation in 2% osmium tetraoxide. After washing, samples were stained with 0.5% uranyl acetate overnight, dehydrated and embedded. Ultrathin slices (70-90 nm) were prepared using an ultramicrotome and examined under transmission electron microscope (FEI, USA).

Co-immunoprecipitation (Co-IP)

Cells were lysed in RIPA buffer supplemented with protease inhibitors. Protein lysates were incubated with anti-SLC7A11 antibody or control IgG overnight at 4°C, followed by incubation with Protein A/G agarose beads to precipitate immune complexes. After washing, the immunoprecipitated proteins were eluted and subjected to Western blot analysis. UFM1-modified SLC7A11 was detected using an anti-UFM1 antibody, while total SLC7A11 levels were assessed using an anti-SLC7A11 antibody.

Western blot analysis

Total proteins were extracted from cells and tumor tissues using RIPA lysis buffer. Equal amounts of protein samples were separated by SDS-PAGE and then transferred onto PVDF membranes. The membranes were blocked with 5% non-fat milk for 1 h at room temperature, followed by overnight incubation at 4°C with primary antibodies against UFM1 (1:1000; ab109305; Abcam, Cambridge, MA, USA), SLC7A11 (1:1000; ab307601; Abcam, Cambridge, MA, USA), and GAPDH (1:5000; ab8245; Abcam, Cambridge, MA, USA). After washing with TBST, membranes were incubated with HRP-conjugated secondary antibodies (1:5000; ab150077; Abcam, Cambridge, MA, USA) for 1 h at room temperature. Protein bands were visualized using an ECL chemiluminescence detection system (Millipore), and band intensities were quantified with ImageJ software.

Xenograft tumor model

28-day-old male BALB/c nude mice were obtained from Beijing Vital River Laboratory

Animal Technology Co., Ltd. Mice were randomly divided into two groups (n = 5 per group) and housed under specific pathogen-free (SPF) conditions with free access to sterilized food and water. Housing condition was maintained at a temperature of 22-25°C, relative humidity of 40%-70%, and a 12 h light/dark cycle. Cal27 cells stably expressing sh-UFM1 or sh-NC were suspended in PBS and subcutaneously injected into the flanks of the mice (1×10^6 cells in 100 μL PBS per mouse). Tumors size was measured weekly using a caliper, and tumor volume was calculated using the formula: volume =(Length × Width^2)/2. At the end of the fourth week, mice were euthanized by CO_2 inhalation followed by cervical dislocation. Tumors were excised, weighed, and processed for further analyses. All animal experiments were approved by the Animal Ethics Committee of Shanxi Provincial People's Hospital.

IHC analysis

Tissue specimens were fixed in 4% Paraformaldehyde, embedded in paraffin, and sectioned at a thickness of 4 μm. Sections were deparaffinized, rehydrated, and subjected to antigen retrieval using citrate buffer (PH 6.0). After blocking with 5% goat serum, the sections were incubated overnight at 4°C with primary antibodies against SLC7A11 (1:200; ab307601; Abcam) and 4-hydroxynonenal (4-HNE; 1:100; ab48506; Abcam). After washing, the sections were incubated with HRP-conjugated secondary antibodies, and immunoreactivity was visualized using DAB as chromogen. Subsequently, sections were counterstained with hematoxylin. Images were captured using an Olympus (Japan) light microscope.

Bioinformatic analysis

The expression profile of UFM1 in HNSC was analyzed using the UALCAN (http://ualcan.path.uab.edu) and GEPIA (http://gepia.cancer-pku.cn) databases. Immunohistochemical profiles of UFM1 in normal oral epithelium and HNSC tissues were further obtained from the Human Protein Atlas (HPA; https://www.proteinatlas.org).

Statistical analysis

Statistical analysis was performed using GraphPad Prism 8.0 software (SanDiego, USA). All results were presented as the mean ± standard deviation (SD). Comparisons between two groups were conducted using an unpaired Student's t-test, while comparisons among multiple groups were performed using one-way ANOVA or two-way ANOVA followed by Tukey's post hoc analysis. For data with repeated measures across time points (e.g., cell proliferation curves and tumor growth curves), repeated measures two-way ANOVA was applied, followed by Tukey's post hoc test for multiple comparisons. A P value < 0.05 was considered statistically significant.

Results

Expression of UFM1 in OSCC

To explore the role of UFM1 in OSCC, we first analyzed its expression profile in HNSC using bioinformatics tools. Analysis of the UALCAN and GEPIA databases revealed that UFM1 mRNA expression was significantly upregulated in HNSC samples compared with normal controls (**Figure 1A**, **1B**). Consistently, qRT-PCR analysis showed that UFM1 expression was significantly upregulated in OSCC tissues compared with their adjacent normal tissues (**Figure 1C**). Furthermore, IHC data from the HPA demonstrated significantly elevated UFM1 protein expression in HNSC tissues compared with normal oral mucosa (**Figure 1D**). In line with these findings, western blot analysis showed that UFM1 protein levels were significantly higher in OSCC cell lines (Scc-25, Cal27, and Ca9-22) than in HOK (**Figure 1E**).

UFM1 knockdown inhibited the malignancy phenotype of OSCC cells

To further explore the functional role of UFM1 in OSCC, specific small interfering RNA targeting UFM1 (si-UFM1) was used to silence UFM1 expression in Cal27 and Ca9-22 cells. Western blot confirmed that UFM1 protein expression was significantly reduced in the si-UFM1 group compared with the negative control group (si-NC) (**Figure 2A**). Functional assays showed that UFM1 knockdown significantly inhibited the malignant phenotype of OSCC cells. Specifically, CCK-8 and colony formation assays showed significant reductions in cell proliferation and clonogenicity after UFM1 knockdown (**Figure 2B**, **2C**). In addition, Transwell assays demonstrated significantly impaired migratory and

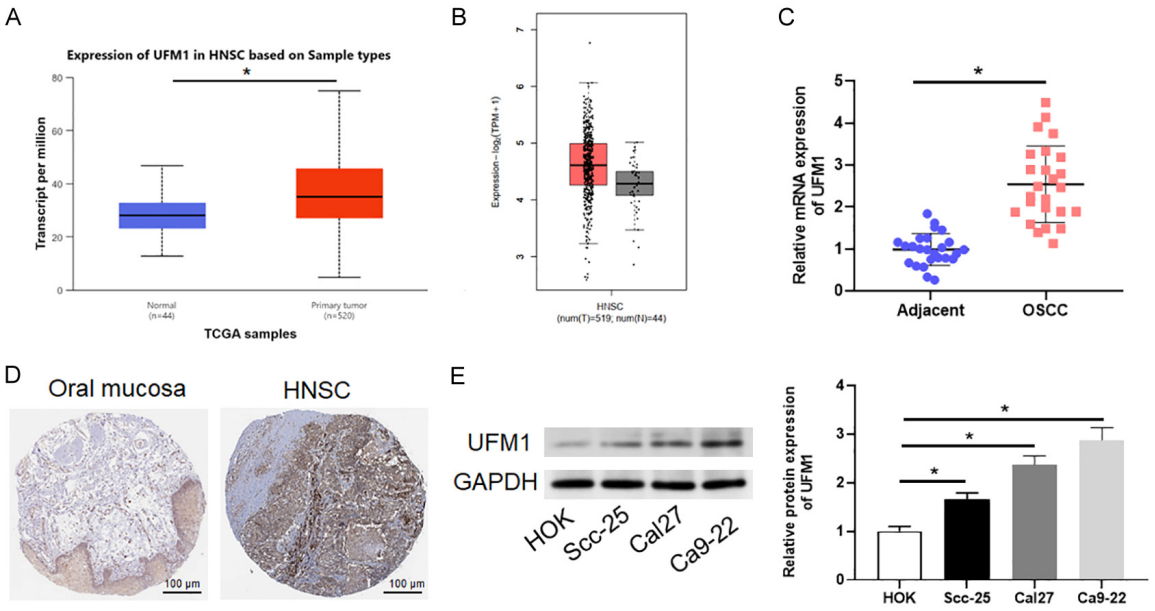

Figure 1. UFM1 is overexpressed in OSCC. (A, B) UFM1 expression in HNSC and normal tissues from UALCAN (A) and GEPIA (B) databases; (C) Validation of UFM1 mRNA upregulation in OSCC clinical specimens by qRT-PCR; (D) Representative IHC images showing UFM1 protein expression in normal oral mucosa and HNSC tissues from the Human Protein Atlas (Scale bars = 100 μm; original magnification: ×100); (E) Western blot analysis of UFM1 protein levels in HOK and OSCC cell lines. *P < 0.05.

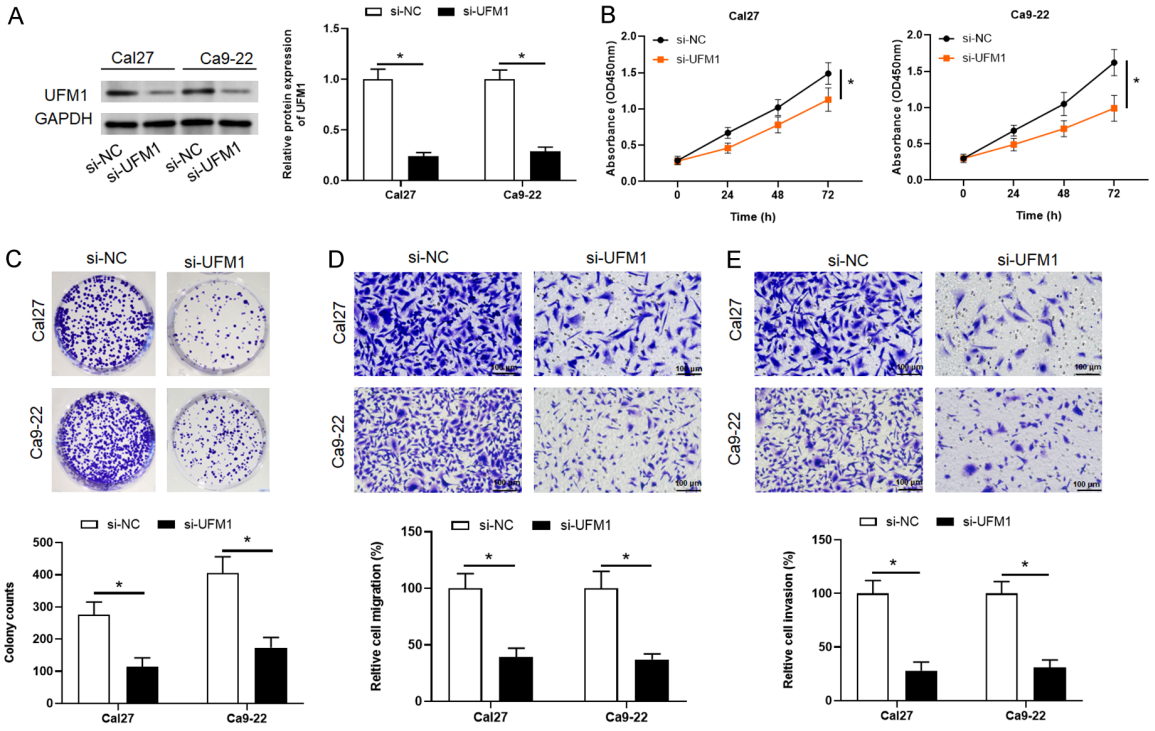

Figure 2. UFM1 knockdown suppressed OSCC cell malignant phenotypes. (A) Western blot analysis showing UFM1 protein levels in Cal27 and Ca9-22 cells after UFM1 depletion; (B) Cell viability curves measured by the CCK-8 assay at indicated time points. (C) Representative images and quantification of colony formation capacity. (D, E) Transwell assays assessing migration (D) and invasion (E) (Scale bars = 100 μm; original magnification: ×100). *P < 0.05.

invasive abilities of OSCC cells following UFM1 knockdown (**Figure 2D**, **2E**).

UFM1 depletion induced ferroptosis in OSCC cells

To determine the type of cell death induced by UFM1 depletion, cells were treated with different inhibitors targeting different cell death pathways. Suppression of Cal27 and Ca9-22 cell viability induced by si-UFM1 was significantly rescued by the ferroptosis inhibitors Liproxstatin-1 and Ferrostatin-1, but not by the apoptosis inhibitor Z-VAD-FMK, the necroptosis inhibitor Nec-1, or the autophagy inhibitor 3-MA, as reflected by comparable cell death rates in the Lip-1 and Fer-1 groups with the control group but persistently elevated cell death rates in the Z-VAD-FMK, Nec-1, and 3-MA groups (**Figure 3A**, **3B**). These findings indicate that ferroptosis is the predominant form of cell death induced by UFM1 knockdown.

Next, we examined the features of ferroptosis and observed that UFM1 knockdown induced significant oxidative stress, characterized by a drop in GSH content and a significant rise in MDA (**Figure 3C**, **3D**). Notably, TEM further revealed characteristic mitochondrial alterations, including reduced mitochondrial size and decreased cristae density in UFM1-deficient cells (**Figure 3E**). Moreover, UFM1 knockdown markedly increased intracellular and mitochondrial ROS levels, as assessed by DCFH-DA and MitoSOX assays, respectively, along with elevated intracellular Fe^{2+} levels (**Figure 3F-J**). Consistently, UFM1 depletion significantly reduced the protein level of SLC7A11, an essential ferroptosis-inhibitory factor (**Figure 3K**), implying that UFM1 might modulate SLC7A11 via post-translational mechanism, potentially through UFMylation-mediated stabilization. These metabolic and ultrastructural alterations demonstrate that UFM1 deficiency causes ferroptotic cell death in OSCC cells.

UFM1 regulates malignant OSCC phenotypes via SLC7A11

Given that SLC7A11 is a key ferroptosis inhibitor and has been reported as a candidate for UFMylation, we assumed that UFM1 exerted its oncogenic effects by stabilizing SLC7A11 at the post-translational level. Consistent with this notion, analysis of public databases (UALCAN) and qRT-PCR both revealed that SLC7A11 expression was significantly upregulated in HNSC and OSCC tissues (**Figure 4A**, **4B**). Furthermore, a significant positive correlation was observed between UFM1 and SLC7A11 expression in HNSC samples (**Figure 4C**).

Co-IP assays further supported the interaction between UFM1 and SLC7A11 (**Figure 4D**). To elucidate this regulatory route, rescue experiments were performed by overexpressing SLC7A11 in UFM1-silenced Cal27 and Ca9-22 cells. Restoration of SLC7A11 successfully rescued the reduced protein levels caused by UFM1 knockdown (**Figure 4E**). Functionally, restoration of SLC7A11 significantly reversed the inhibitory effects of UFM1 depletion on cell proliferation, clonogenicity, migration and invasion (**Figure 4F-H**). These results indicate that SLC7A11 acts as an important down-stream effector of UFM1 in promoting OSCC.

SLC7A11 overexpression attenuated UFM1 deficiency-induced ferroptotic stress

To further verify that UFM1 regulates ferroptosis via SLC7A11, we investigated whether SLC7A11 overexpression could reverse the oxidative stress and metabolic disorders induced by UFM1 knockdown. In both Cal27 and Ca9-22 cells, SLC7A11 overexpression effectively relieved the oxidative stress and metabolic disorder induced by si-UFM1. Specifically, SLC7A11 overexpression significantly suppressed intracellular ROS, mitochondrial superoxide, MDA, and ferrous iron levels (**Figure 5A-D**), while restoring the decreased GSH levels (**Figure 5E**). Importantly, CCK-8 experiments showed that SLC7A11 overexpression significantly alleviated the reduction in cell viability caused by UFM1 silencing (**Figure 5F**). Thus, these findings suggest that SLC7A11 acts as an indispensable downstream effector mediating UFM1-dependent protection against ferroptosis in OSCC cells.

UFM1 knockdown suppressed tumor growth and modulated SLC7A11 expression in vivo

To evaluate the tumorigenic potential of UFM1 in vivo, a xenograft mouse model was established using Cal27 cells stably expressing sh-UFM1 or sh-NC. Knockdown of UFM1 significantly suppressed tumor growth compared with the control group (**Figure 6A-C**). Consistent

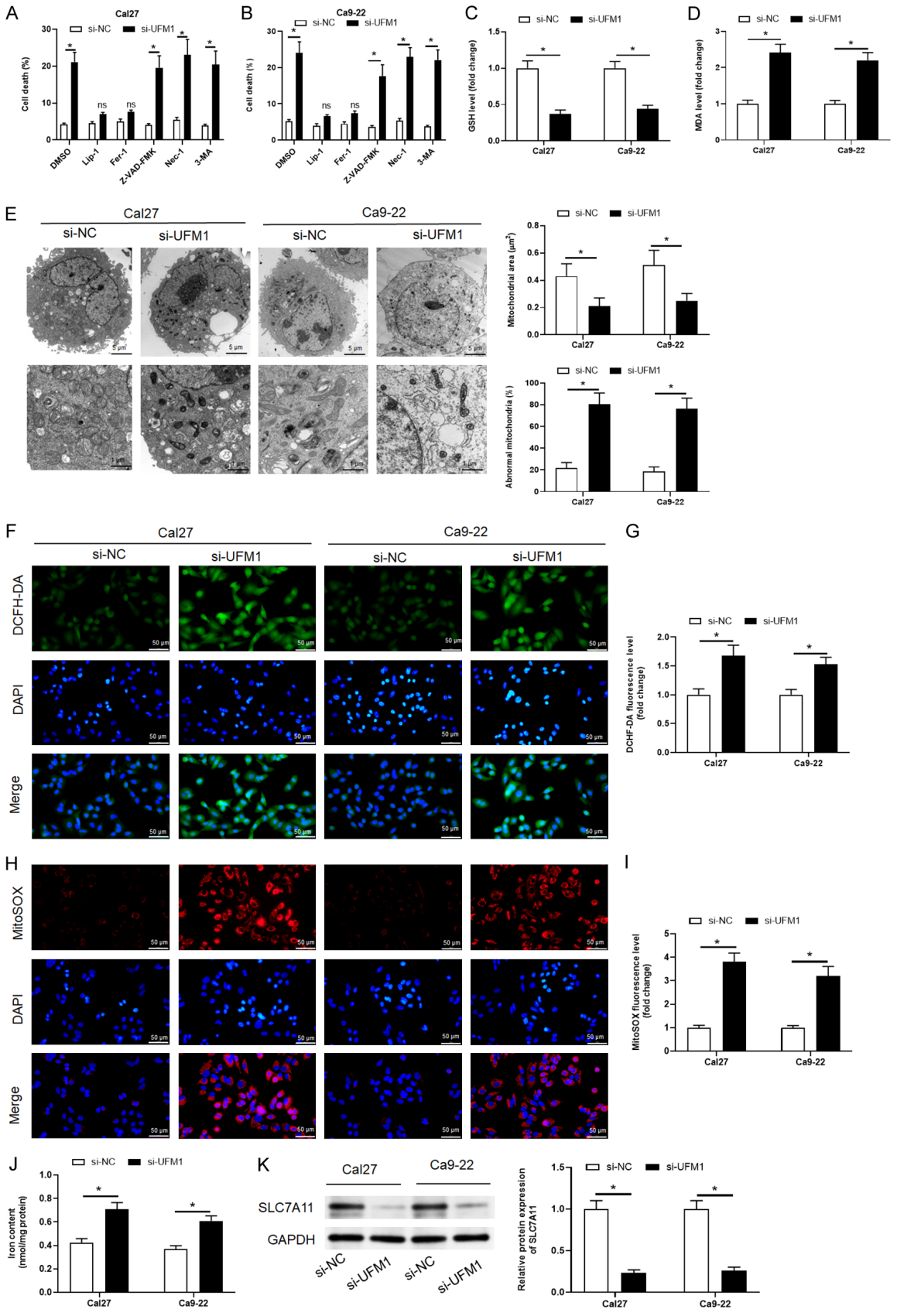

Figure 3. UFM1 deficiency triggers ferroptosis in OSCC cells. (A, B) Cell viability of UFM1-knockdown cells treated with different cell death inhibitors (Fer-1: Ferrostatin-1; Lip-1: Liproxstatin-1; Z-VAD: pan-caspase inhibitor; Nec-

1: Necrostatin-1; 3-MA: autophagy inhibitor). (C) Quantification of intracellular GSH content. (D) Measurement of lipid peroxidation by MDA assay. (E) TEM images showing characteristic ferroptotic mitochondrial morphology (Scale bar = 5 μm or 1 μm; original magnification: ×2000 or ×1000). (F-J) Detection of intracellular ROS (F, G) and mitochondrial superoxide levels (H, I) using DCFH-DA and MitoSOX Red probes, respectively (Scale bar = 50 μm; original magnification: ×200); (J) Intracellular ferrous iron levels. (K) Western blot analysis of SLC7A11. *P < 0.05.

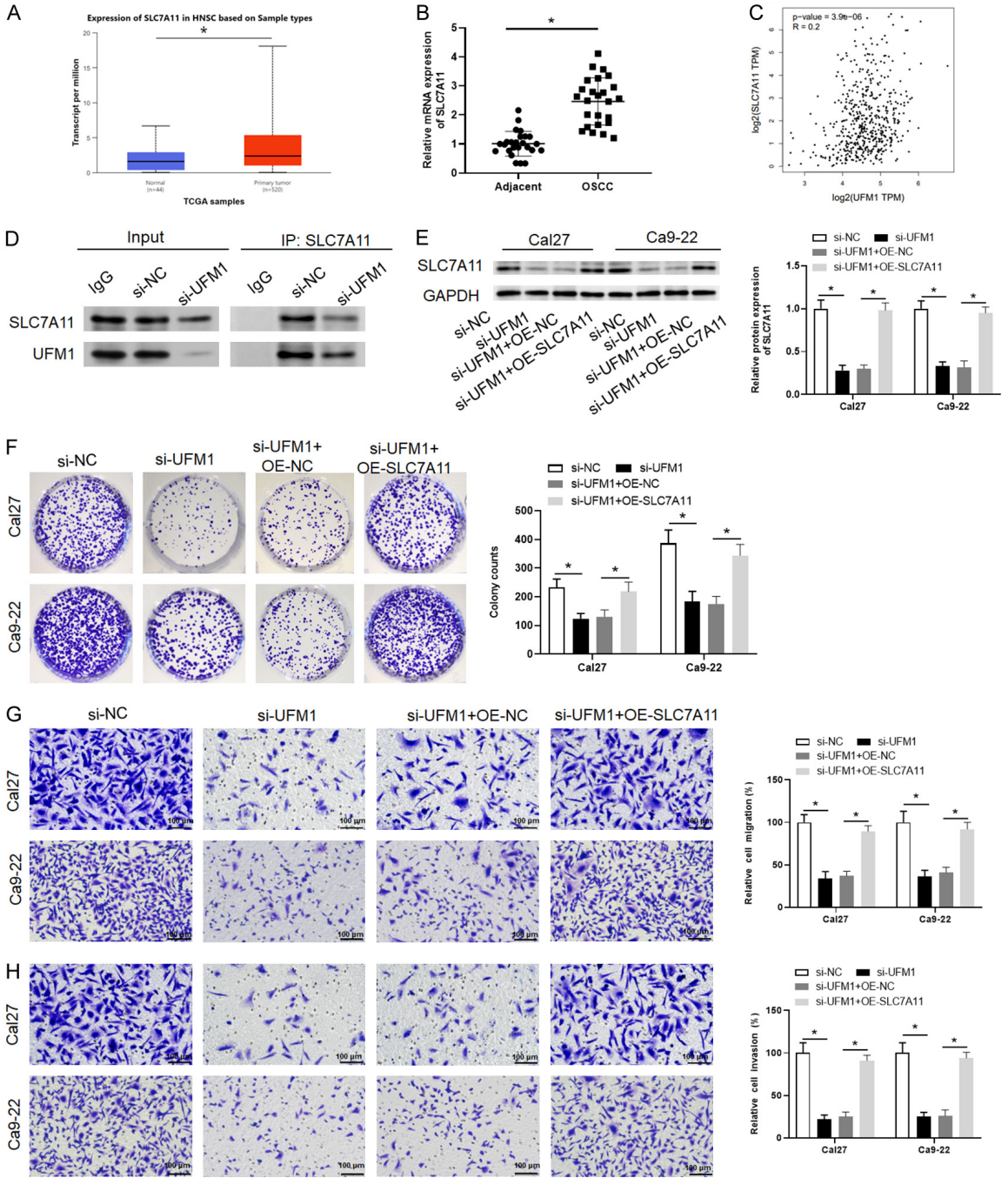

Figure 4. SLC7A11 mediated the oncogenic effects of UFM1 in OSCC. (A) SLC7A11 mRNA expression levels in HNSC tissues from the UALCAN database; (B) Validation of SLC7A11 mRNA upregulation in OSCC specimens by qRT-PCR; (C) Positive correlation between UFM1 and SLC7A11 mRNA expression in HNSC samples from GEPIA database; (D) Co-IP analysis showing the interaction between SLC7A11 and UFM1; (E) Western blot analysis showing restoration of SLC7A11 protein expression upon ectopic overexpression in UFM1-knockdown cells; (F-H) Functional rescue assays demonstrating that SLC7A11 overexpression reverses the suppressive effects of UFM1 knockdown on clonogenic survival (F), cell migration (G), and invasion (H) (Scale bars = 100 μm; original magnification: ×100). *P < 0.05.

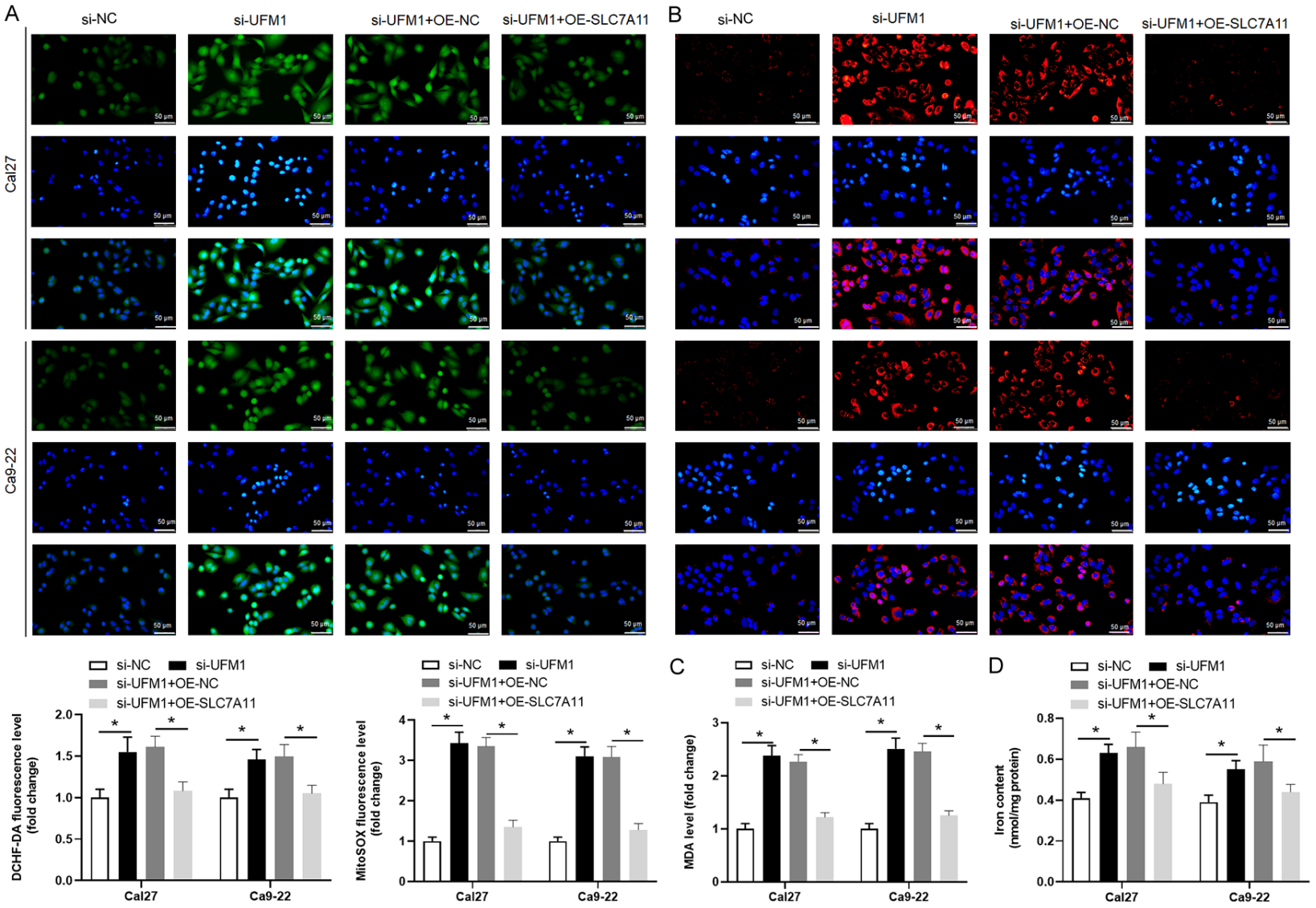
A
si-NC
si-UFM1
si-UFM1+OE-NC
si-UFM1+OE-SLC7A11
Cal27
Ca9-22
50 μm
B
si-NC
si-UFM1
si-UFM1+OE-NC
si-UFM1+OE-SLC7A11
C
si-NC
si-UFM1
si-UFM1+OE-NC
si-UFM1+OE-SLC7A11
DCHF-DA fluorescence level (fold change)
MitoSOX fluorescence level (fold change)
MDA level (fold change)
Cal27
Ca9-22
D
si-NC
si-UFM1
si-UFM1+OE-NC
si-UFM1+OE-SLC7A11
Iron content (nmol/mg protein)
Cal27
Ca9-22

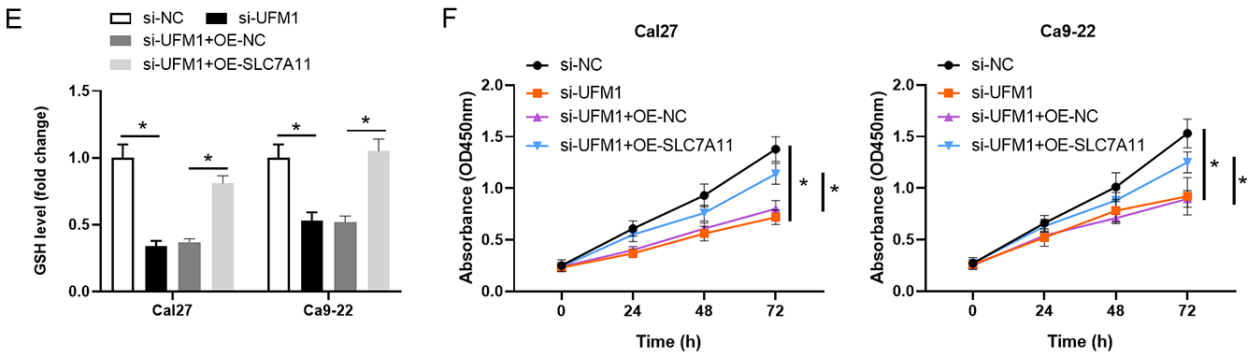

Figure 5. SLC7A11 overexpression attenuates UFM1 knockdown-induced ferroptotic events. A. Intracellular ROS levels detected by DCFH-DA fluorescence (Scale bar = 50 μm; original magnification: ×200); B. Mitochondrial superoxide production measured by MitoSOX Red staining (Scale bar = 50 μm; original magnification: ×200); C. Lipid peroxidation assessed by MDA content; D. Cellular ferrous iron levels; E. Measurement of glutathione (GSH) level; F. Cell viability assessed by the CCK-8 assay. *P < 0.05.

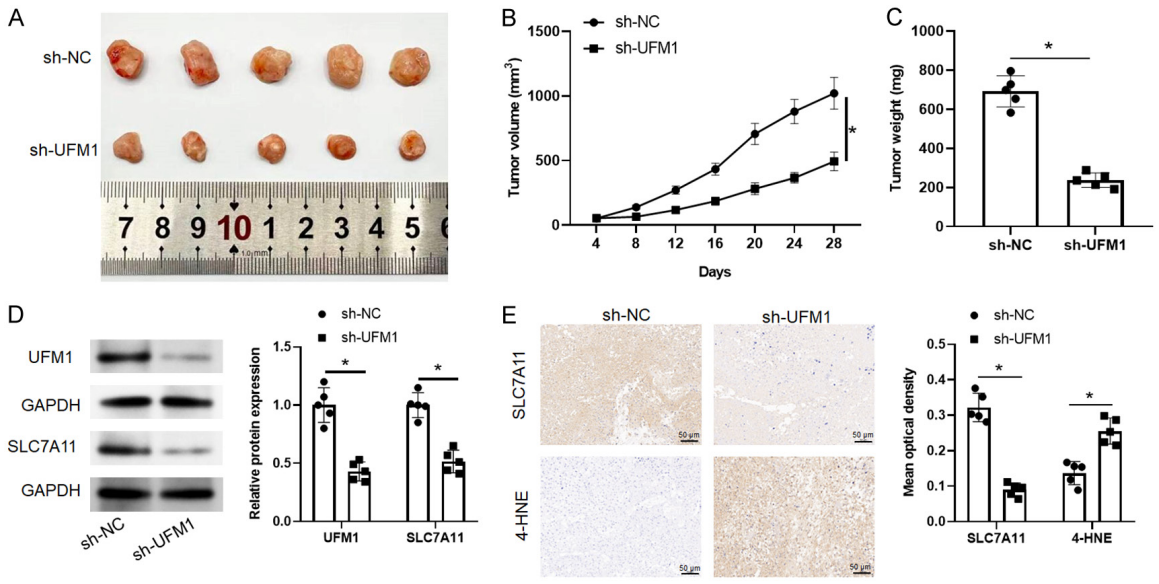

Figure 6. UFM1 knockdown attenuates tumor growth in vivo. (A) Tumors resected from nude mice at the end point of experiment; (B, C) Tumor growth curves (B) and final tumor weights (C) measured after 4 weeks of treatment (n=5 mice per group); (D) Western blot analysis of UFM1 and SLC7A11 protein expression in tumor tissues from different groups; (E) Representative IHC staining images and quantification of SLC7A11 and 4-HNE in tumor tissues (Scale bar = 50 μm; original magnification: ×200). *P < 0.05.

with the *in vitro* findings, Western blotting on excised tumor tissues revealed that both UFM1 and SLC7A11 protein levels were markedly decreased in the sh-UFM1 group (**Figure 6D**). Moreover, IHC analysis showed that SLC7A11 expression was significantly reduced in tumors derived from sh-UFM1 cells. In contrast, the expression of 4-hydroxynonenal (4-HNE), an indicator of lipid peroxidation, was significantly upregulated in sh-UFM1 groups (**Figure 6E**), indicating significantly enhanced ferroptosis in vivo.

Discussion

This study demonstrates that UFM1 acts as a key oncogenic factor during OSCC progression. Our results indicated that UFM1 promoted OSCC progression by stabilizing SLC7A11, conferring resistance against ferroptotic cell death.

UFM1-mediated UFMylation exerts context-dependent effects on downstream targets [23]. In colorectal cancer, UFM1 has been reported to modify BAP1, thereby enhancing oncogenic signaling associated with pVHL [24]. Additionally, UFM1 can promote immune evasion through PLAC8- mediated upregulation of PD-L1 [25]. In breast cancer, UFM1 interacts with ASC1 to activate estrogen receptor α (ERα) signaling [14]. In pancreatic ductal adenocarcinoma, UFM1 suppresses ferroptosis by inhibiting GPX4 transcription [15]. Notably, metformin was reported to suppress ferroptosis in breast cancer through inhibition of UFM1-mediated UFMylation of SLC7A11, thereby preserving redox homeostasis [22].

Consistent with previous reports [16, 26], this study revealed a significant upregulation of UFM1 in both OSCC and HNSC tissues and cell lines. Mechanistically, our findings demonstrated that UFM1 depletion induced ferroptosis in OSCC cells, characterized by increased ROS, lipid peroxidation, Fe^{2+} accumulation, and reduced GSH and SLC7A11 expression. Furthermore, targeted rescue experiments using ferroptosis blockers (Liproxstatin-1, Ferrostatin-1) partially reversed the effects of UFM1 knockdown, supporting the involvement of ferroptosis in this process. Our results also demonstrated that UFM1 knockdown significantly suppressed OSCC cell proliferation, migration, invasion, and tumorigenesis, highlighting the pro-tumorigenic role of UFM1 in OSCC.

SLC7A11 is a key regulator of ferroptosis. Accumulating evidence has elucidated the reg-

ulatory network governing SLC7A11 in OSCC. Xu et al. reported that SLC7A11 mRNA stability is regulated by METTL3, an m^6A methyltransferase, and its depletion leads to reduced SLC7A11 expression and suppression of malignant phenotypes in OSCC cells [27]. In addition, Liu et al. demonstrated that the deubiquitinase OTUB1 inhibits ferroptosis by reducing the ubiquitination of SLC7A11, thereby enhancing OSCC resistance to cisplatin [28]. Zhou et al. showed that SLC7A11 knockdown effectively suppressed OSCC cell growth through induction of ferroptosis [21].

In the present study, we demonstrated that UFM1 promoted OSCC progression by regulating SLC7A11 at the post-translational level. Co-IP revealed a potential interaction between UFM1 and SLC7A11, suggesting that UFM1-mediated UFMylation may stabilize SLC7A11, potentially protecting SLC7A11 from degradation by the proteasome or lysosome. Rescue assays further indicated that restoration of SLC7A11 effectively counteracted UFM1 depletion-induced ferroptosis and malignant phenotypic alterations. These findings are consistent with previous reports in breast cancer, in which UFMylation of SLC7A11 was shown to inhibit ferroptosis [22], suggesting that this regulatory axis may be conserved across multiple cancer types.

Despite the evidence presented in this study supporting a role for UFM1 in promoting OSCC progression through stabilization of SLC7A11 and suppression of ferroptosis, several limitations should be acknowledged. First, the upstream regulatory mechanisms that activate the UFM1/SLC7A11 pathway in OSCC remains unclear. Second, the precise molecular mechanism by which UFM1 maintains SLC7A11 protein stability has not been fully elucidated. Future studies should focus on identifying the specific UFMylation sites on SLC7A11 and investigating whether this modification directly affects SLC7A11 degradation, as well as exploring the upstream factors that drive the activation of UFM1/SLC7A11 axis in OSCC.

Conclusion

UFM1 acts as a key regulator of OSCC progression by modulating SLC7A11-mediated resistance to ferroptosis. These findings provide new insights into the role of UFMylation in cancer biology, offering novel therapeutic target for OSCC.

Disclosure of conflict of interest

None.

Address correspondence to: Gang Li, Department of Prosthodontics, Shanxi Provincial People's Hospital, No. 29 Shuangtasi Street, Yingze District, Taiyuan 030012, Shanxi, China. E-mail: 18635132603@163.com

References

[1] Hutchens T, Thorstad W, Wang X, Li Y, Duncavage EJ, Sun L and Chernock RD. Head and neck squamous cell carcinomas of unknown primary: can ancillary studies help identify more primary tumor sites? Exp Mol Pathol 2024; 138: 104915.

[2] Sung H, Ferlay J, Siegel RL, Laversanne M, Soerjomataram I, Jemal A and Bray F. Global cancer statistics 2020: GLOBOCAN estimates of incidence and mortality worldwide for 36 cancers in 185 countries. CA Cancer J Clin 2021; 71: 209-249.

[3] Tan Y, Wang Z, Xu M, Li B, Huang Z, Qin S, Nice EC, Tang J and Huang C. Oral squamous cell carcinomas: state of the field and emerging directions. Int J Oral Sci 2023; 15: 44.

[4] Lee DS, Ramirez RJ, Lee JJ, Valenzuela CV, Zevallos JP, Mazul AL, Puram SV, Doering MM, Pipkorn P and Jackson RS. Survival of young versus old patients with oral cavity squamous cell carcinoma: a meta-analysis. Laryngoscope 2021; 131: 1310-1319.

[5] Zhou Y, Wang L, Liu M, Jiang H and Wu Y. Oral squamous cell carcinoma: insights into cellular heterogeneity, drug resistance, and evolutionary trajectories. Cell Biol Toxicol 2025; 41: 101.

[6] Komatsu M, Inada T and Noda NN. The UFM1 system: working principles, cellular functions, and pathophysiology. Mol Cell 2024; 84: 156-169.

[7] Wang X, Lv X, Ma J and Xu G. UFMylation: an integral post-translational modification for the regulation of proteostasis and cellular functions. Pharmacol Ther 2024; 260: 108680.

[8] DaRosa PA, Penchev I, Gumbin SC, Scavone F, Wąchalska M, Paulo JA, Ordureau A, Peter JJ, Kulathu Y, Harper JW, Becker T, Beckmann R and Kopito RR. UFM1 E3 ligase promotes recycling of 60S ribosomal subunits from the ER. Nature 2024; 627: 445-452.

[9] Lee L, Perez Oliva AB, Martinez-Balsalobre E, Churikov D, Peter J, Rahmouni D, Audoly G, Az-

zoni V, Audebert S, Camoin L, Mulero V, Cayuela ML, Kulathu Y, Geli V and Lachaud C. UFMylation of MRE11 is essential for telomere length maintenance and hematopoietic stem cell survival. Sci Adv 2021; 7: eabc7371.

[10] Nahorski MS, Maddirevula S, Ishimura R, Alsahli S, Brady AF, Begemann A, Mizushima T, Guzmán-Vega FJ, Obata M, Ichimura Y, Alsaif HS, Anazi S, Ibrahim N, Abdulwahab F, Hashem M, Monies D, Abouelhoda M, Meyer BF, Alfadhel M, Eyaid W, Zweier M, Steindl K, Rauch A, Arold ST, Woods CG, Komatsu M and Alkuraya FS. Biallelic UFM1 and UFC1 mutations expand the essential role of ufmylation in brain development. Brain 2018; 141: 1934-1945.

[11] Yan T, Heckman MG, Craver EC, Liu CC, Rawlinson BD, Wang X, Murray ME, Dickson DW, Ertekin-Taner N, Lou Z, Bu G, Springer W and Fiesel FC. The UFMylation pathway is impaired in Alzheimer's disease. Mol Neurodegener 2024; 19: 97.

[12] Jing J, Yang F, Wang K, Cui M, Kong N, Wang S, Qiao X, Kong F, Zhao D, Ji J, Tang L, Gao J, Cong YS, Ding D and Chen K. UFMylation of NLRP3 prevents its autophagic degradation and facilitates inflammasome activation. Adv Sci (Weinh) 2025; 12: e2406786.

[13] Chung CH and Yoo HM. Emerging role of protein modification by UFM1 in cancer. Biochem Biophys Res Commun 2022; 633: 61-63.

[14] Yoo HM, Kang SH, Kim JY, Lee JE, Seong MW, Lee SW, Ka SH, Sou YS, Komatsu M, Tanaka K, Lee ST, Noh DY, Baek SH, Jeon YJ and Chung CH. Modification of ASC1 by UFM1 is crucial for ERα transactivation and breast cancer development. Mol Cell 2014; 56: 261-274.

[15] Li G, Liao C, Chen J, Wang Z, Zhu S, Lai J, Li Q, Chen Y, Wu D, Li J, Huang Y, Tian Y, Chen Y and Chen S. Targeting the MCP-GPX4/HMGB1 axis for effectively triggering immunogenic ferroptosis in pancreatic ductal adenocarcinoma. Adv Sci (Weinh) 2024; 11: e2308208.

[16] Derfi KV, Vasiljevic T, Dragicevic T and Glavan TM. Mithramycin targets head and neck cancer stem cells by inhibiting Sp1 and UFMylation. Cancer Cell Int 2024; 24: 412.

[17] Dixon SJ, Lemberg KM, Lamprecht MR, Skouta R, Zaitsev EM, Gleason CE, Patel DN, Bauer AJ, Cantley AM, Yang WS, Morrison B 3rd and Stockwell BR. Ferroptosis: an iron-dependent form of nonapoptotic cell death. Cell 2012; 149: 1060-1072.

[18] Rodriguez R, Schreiber SL and Conrad M. Persister cancer cells: iron addiction and vulnerability to ferroptosis. Mol Cell 2022; 82: 728-740.

[19] He F, Zhang P, Liu J, Wang R, Kaufman RJ, Yaden BC and Karin M. ATF4 suppresses hepatocarcinogenesis by inducing SLC7A11 (xCT) to block stress-related ferroptosis. J Hepatol 2023; 79: 362-377.

[20] Jiao R and Long H. Ferroptosis: a new challenge and target in oral diseases. Oral Dis 2025; 31: 1626-1636.

[21] Zhou R, Zhou J, Xiong Y, Su K, Liu C, Cheng B and Wu T. Sulfasalazine combined with anti-IL-1β mAb induces ferroptosis and immune modulation in oral squamous cell carcinoma. Cell Mol Life Sci 2025; 82: 216.

[22] Yang J, Zhou Y, Xie S, Wang J, Li Z, Chen L, Mao M, Chen C, Huang A, Chen Y, Zhang X, Khan NUH, Wang L and Zhou J. Metformin induces Ferroptosis by inhibiting UFMylation of SLC7A11 in breast cancer. J Exp Clin Cancer Res 2021; 40: 206.

[23] Liu J, Guan D, Dong M, Yang J, Wei H, Liang Q, Song L, Xu L, Bai J, Liu C, Mao J, Zhang Q, Zhou J, Wu X, Wang M and Cong YS. UFMylation maintains tumour suppressor p53 stability by antagonizing its ubiquitination. Nat Cell Biol 2020; 22: 1056-1063.

[24] Yang X, Wen Y, Qin S, Zhou Y, Zhang C, Huang L, Li M, Ma X, Wan R, Chen J, He RR, Gao H, Goding CR, Luo OJ, Shen X, Cui R and Liu T. UFMylation maintains tumor suppressor pVHL stability by activating the deubiquitinase BAP1. Sci Adv 2025; 11: eadt8800.

[25] Mao M, Chen Y, Yang J, Cheng Y, Xu L, Ji F, Zhou J, Zhang X, Li Z, Chen C, Ju S, Zhang J and Wang L. Modification of PLAC8 by UFM1 affects tumorous proliferation and immune response by impacting PD-L1 levels in triple-negative breast cancer. J Immunother Cancer 2022; 10: e005668.

[26] Ke D, Guo HH, Jiang N, Shi RS and Fan TY. Inhibition of UFM1 expression suppresses cancer progression and is linked to the dismal prognosis and immune infiltration in oral squamous cell carcinoma. Aging (Albany NY) 2023; 15: 13059-13076.

[27] Xu L, Li Q, Wang Y, Wang L, Guo Y, Yang R, Zhao N, Ge N, Wang Y and Guo C. m(6)A methyltransferase METTL3 promotes oral squamous cell carcinoma progression through enhancement of IGF2BP2-mediated SLC7A11 mRNA stability. Am J Cancer Res 2021; 11: 5282-5298.

[28] Liu Y, Bai Q, Pang N and Xue J. TCF12 induces ferroptosis by suppressing OTUB1-mediated SLC7A11 deubiquitination to promote cisplatin sensitivity in oral squamous cell carcinoma. Cell Biol Int 2024; 48: 1649-1663.